CHAPTER VI
RESULTS AND DISCUSSION

4.1 Synthesis of cubic *Ia-3d* mesoporous silica

4.1.1 The physico-chemical properties of sulfonic functionalized MCA synthesized by hydrothermal method

4.1.1.1 XRD results

From the XRD patterns of the as-synthesized, extracted and oxidized materials which were synthesized by hydrothermal methods with gel composition 1.0 TEOS: 0.089 MPTMS: 2.0 P123: 2.0 HCl: 148 H_2O was showed in **Figure 4.1**. The XRD pattern of cubic mesoporous material *Ia-3d* showed 2 diffraction peaks, (211) and (220) in the range of 2Θ = 0.7-3.0° with high periodic orderness of mesoporosity and excellent textural uniformity [57]. The extraction with 0.37 M HCl in ethanol could increase the crystallinity because the structure directing agent (Pluronic P123) was removed from the silica framework. Moreover, the cubic structure was not distorted by extraction and oxidation with H_2O_2. In comparison with MCAex, the diffraction peaks of sulfonic functionalized MCAox materials were slightly shifted to higher 2 theta values. It can be indicated that the presence of bulky functional group propyl sulfonic acid, which is lager than propyl thiol groups, on the surface of MCAox decreased pore volume. Furthermore, the crystallinity of MCAox showed lower intensity compare with MCAex because of incorporated organic group into mesoporous materials.

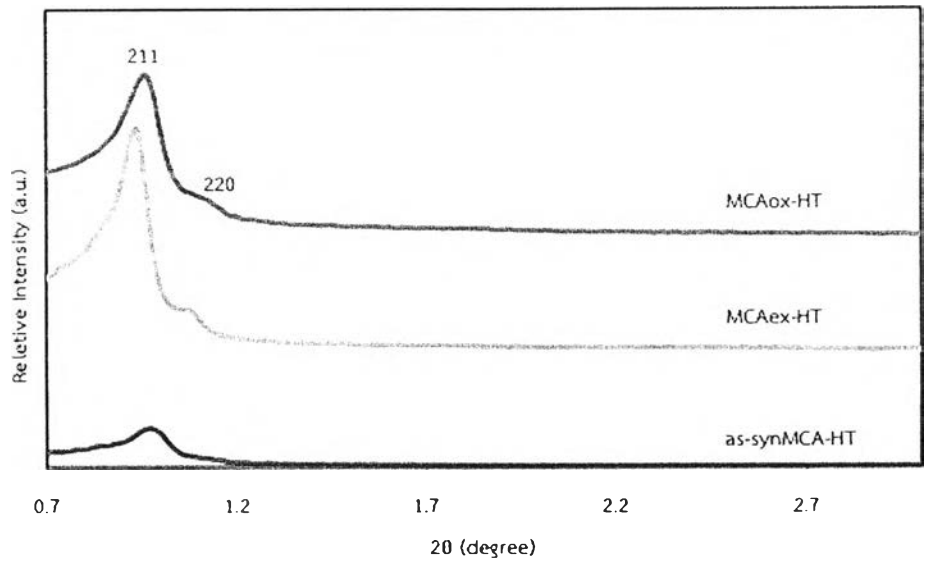

Figure 4.1 XRD patterns of as-synthesized, extracted and oxidized MCA which synthesized by hydrothermal method.

4.1.1.2 Sorption properties

The N_2 adsorption-desorption isotherms of MCAex and MCAox from hydrothermal synthesized materials showed the characteristic isotherm type IV which exhibited a well-defined H1 hysteresis loop according to the IUPAC classification relative to the mesoporous materials (shown in **Figure 4.2-4.3**). The hysteresis loop type H1 associated with pores consisting of agglomerates or compacts of uniform spherical particles with regular array, whose pore size distribution are normally narrow. The corresponding physical properties obtained from N_2 adsorption-desorption analysis are listed in **Table 4.1**. The total specific surface area of MCAex-HT and MCAox-HT were calculated using Brunaure, Emmett and Teller (BET) equation. It can be found that removing structure directing agent from synthesized catalysts gives increasing of surface areas from 558.4 m^2/g to 603.9 m^2/g, for extracted and oxidized samples. In part of pore size distribution, Barrett-Joiner-Halenda (BJH) method was used to evaluate the synthetic materials. The narrow pore size distribution was found in MCAex and MCAox at same the pore diameter of 5.4 nm. Nevertheless, peak distribution of MCAox was broader than MCAex, it can explain that organo sulfonic functional transfer into pore structure that was

corresponding with their intensity of XRD pattern results. Furthermore, it also induced decreasing of pore volume.

Table 4.1 Textural properties of synthesized materials by hydrothermal method.

Catalyst	S_{BET} $(m^2 g^{-1})^a$	Pore volume $(cm^3 g^{-1})^b$	Pore diameter (nm)[b]	a_0 (nm)[c]	Wall thickness (nm)[d]
MCAex-HT	558.4	0.7	5.4	23.1	10.9
MCAox-HT	603.9	0.6	5.4	22.5	10.5

[a] BET specific surface area.

[b] Calculated by using the BJH method

[c] a_0 : cell parameter calculated from $a_o = \sqrt{6} \times d$ where d is d-spacing of the (211) reflection plane from XRD method

[d] wall thickness $T_{wall} = a_0 \sqrt{2}/2 - d_{pore}$, where d_{pore} and a_0 are pore distribution and cubic unit cell parameter respectively [58]

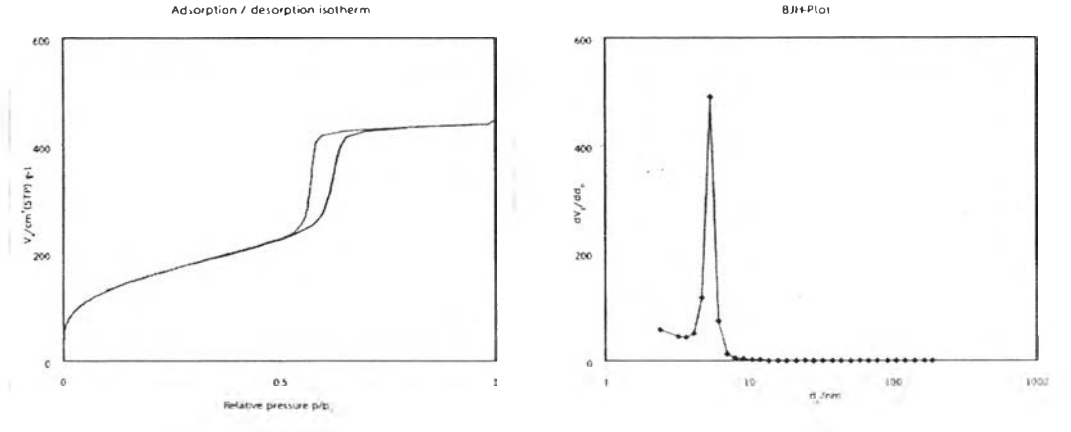

Figure 4.2 N_2 adsorption-desorption isotherm and BJH-pore size distribution of MCAex synthesized by hydrothermal method.

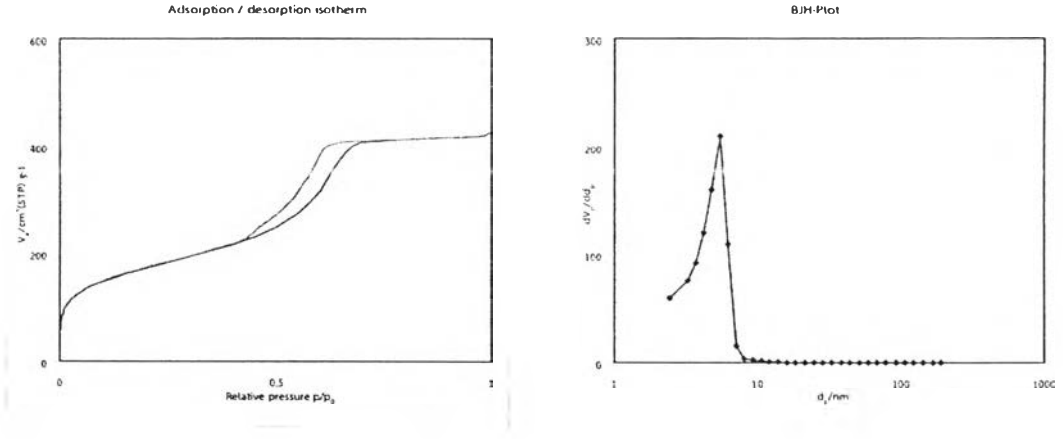

Figure 4.3 N_2 adsorption desorption isotherm and BJH-pore size distribution of MCAox synthesized by hydrothermal method.

4.1.1.3 SEM images

The SEM images of MCAex and MCAox synthesized from hydrothermal are shown in **Figure 4.4**. It can be observed, morphology of MCAex and MCAox were different in particle shape with similar to stone. The size of partical was in range between 50-100 μm. The morphology of MCAox did not change when oxidized with hydrogen peroxide but the particle size distribution was smaller than extracted materials.

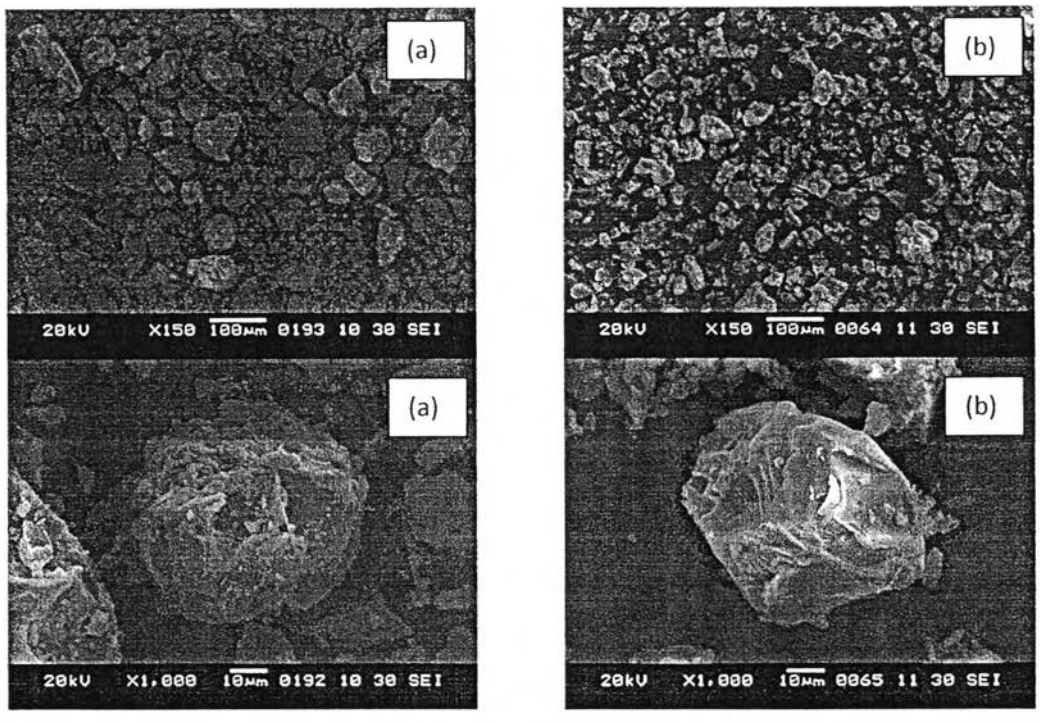

Figure 4.4 SEM images of (a) MCAex and (b) MCAox synthesized by hydrothermal method.

4.1.1.4 TEM images

The TEM images of hydrothermal sulfonic MCAox in cross section view (Figure 4.5) performed well ordered cubic mesostructure with three dimensional channels that confirmed by the longitudinal section view image and indicated the regular arrangement of mesochannels. The cross section images were used to measure the pore size of materials at lattice plane (100) and it is about 4.3 nm.

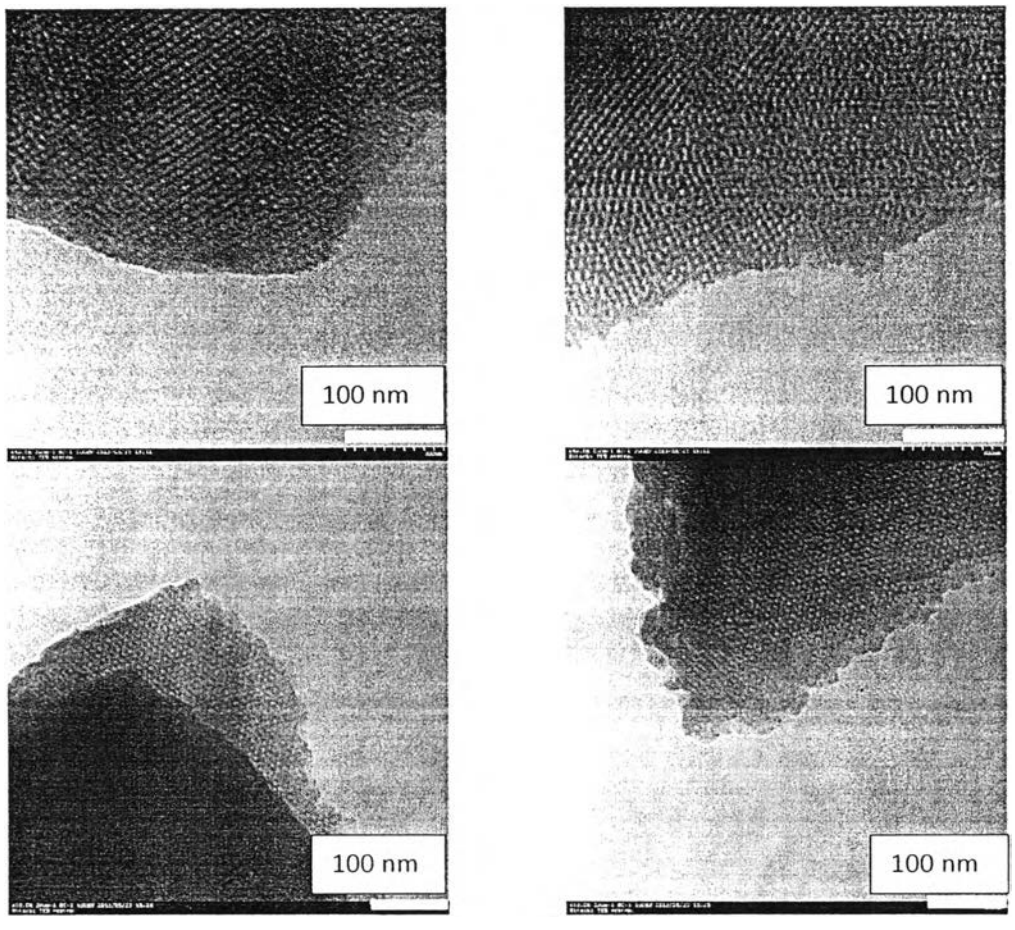

Figure 4.5 TEM images of MCAox synthesized by hydrothermal method.

4.1.2 Effect of crystallization time

XRD patterns of MCAox with crystallization times from 24 hr. and 48 hr., which the gel composition was 1.0 TEOS: 0.089 MPTMS: 2.0 P123: 2.0 HCl: 148 H_2O, were shown in Figure 4.6. At 24 hr., the XRD pattern was occurred at 2θ higher than 48 hr., which can explained by Bragg's rule that the unit cell parameter of materials synthesized at 24 hr. was smaller than 48 hr. The received amount of materials from both of various crystallization times is insignificantly different but at 24 hr. will be slightly higher than 48 hr. because of low density.

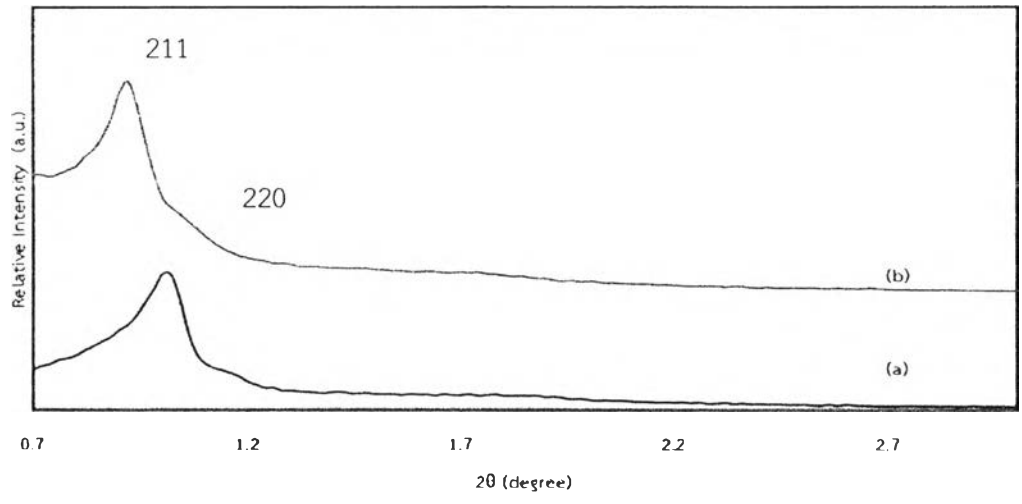

Figure 4.6 XRD patterns of MCAox synthesized by hydrothermal method with different crystallization time (a) 24 hr. and (b) 48 hr.

4.1.3 Effect of aging temperature

The study effect of aging temperature (40, 60 and 80°C) (fig.4.7) found that increasing of aging temperature led to rising of hydrophobicity of EO block in structure directing agent and hydrophobic volume [59]. The XRD patterns of both aging temperature 60° and 80° showed the diffraction peaks (211) and (200) at 0.8-1.2 degree and the broad peaks (321), (400), (420) and (332) at 1.4-2.3 degree which are characteristic peaks of cubic *Ia-3d* mesostructure, showed in **Figure 4.7**. XRD patterns of extracted and oxidized are shifted to lower 2θ, indicating that enlargement of pore size distribution. It can be explained that increasing aging temperatures, polypropylene oxide chains, which aggregated to micelle core PPO blocks in solution, are stretched caused by reduced hydrogen interaction between micelle and water, showed in **Figure 4.8**. Moreover, number of polar state was increased by water become a worse solvent that lead to decrease the crystallinity of material [60, 61].

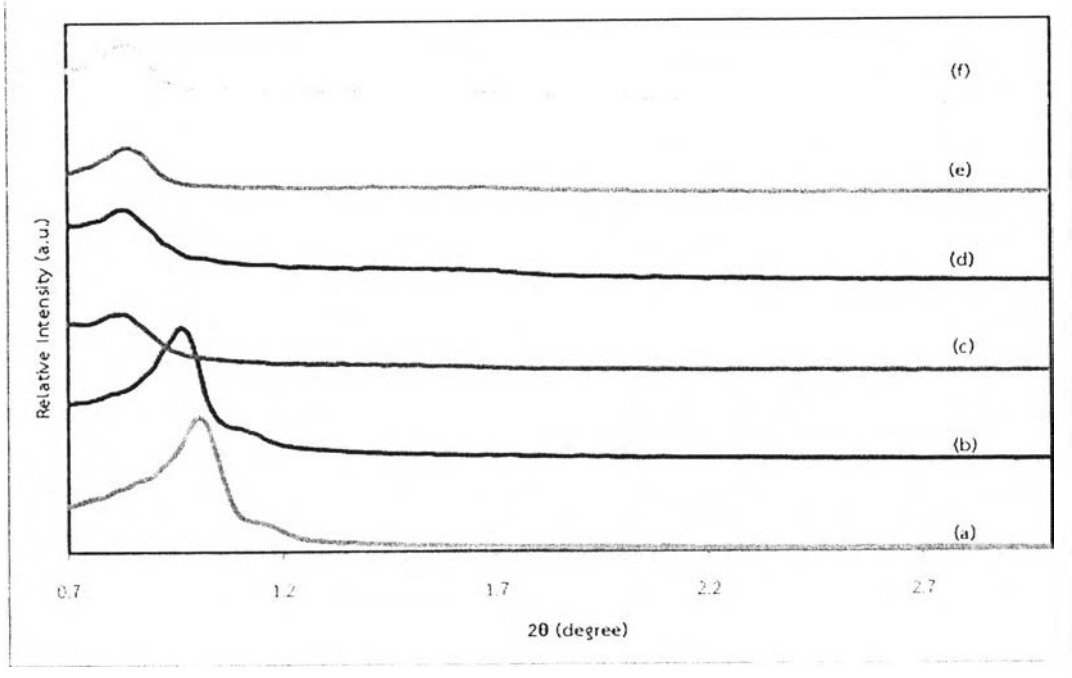

Figure 4.7 XRD patterns of extracted and oxidized catalyst with varied aging temperature (a) MCAex-40, (b) MCAox-40, (c) MCAex-60, (d) MCAox-60, (e) MCAex-80 and (f) MCAox-80.

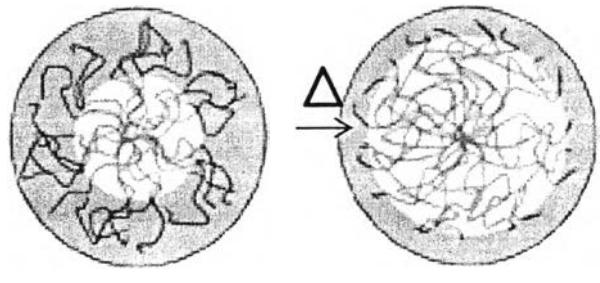

Figure 4.8 The expanding of hydrophobic core PPO block when increasing aging temperature.

The SEM images of oxidized materials with various aging temperature from 40°C-80°C were showed in **Figure 4.9**. To increase aging temperature leads to rise of particle size. The crystallization was not good when using high temperature and it can be seen that the surface of the particle was not smooth.

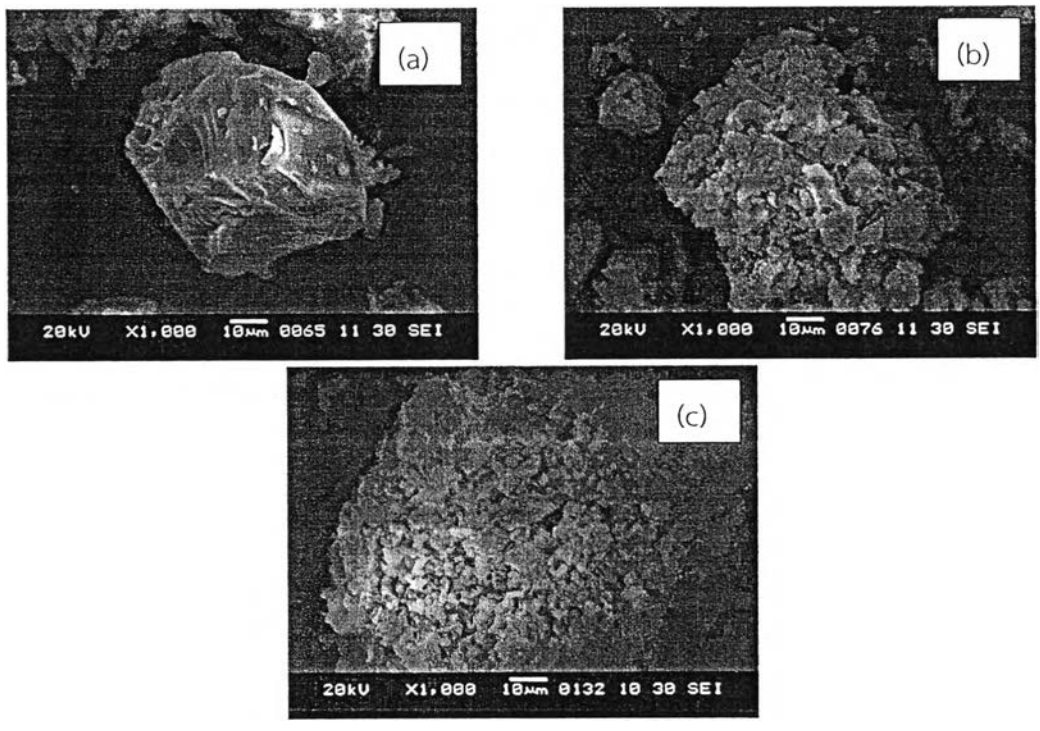

Figure 4.9 SEM images of MCAox synthesized by hydrothermal method varied aging temperature (a) 40°C, (b) 60°C and (c) 80°C.

4.1.4 Effect of amount of Si sources (MPTMS and TEOS)

TEOS and MPTMS were used as silicon sources in this study by varied mole ratio in the range of 1.089 - *x* TEOS and *x* MPTMS when *x* was 0.045-0.179 mol. From the XRD patterns of MCAex-HT with two silicon sources mol ratio with crystallization time48 hr. (**Figure 4.10**), in the synthesis procedure the amount of added MPTMS to the template solution is very important to obtain the ordered *Ia-3d* cubic structure. if amount of MPTMS is added equal or less than 0.067 mol, the ordered 2d-hexagonal SBA-15, with characteristic diffraction peaks (100), (110) and (200), was obtained. When the amount of MPTMS is added in range of 0.067-0.089 mol. the characteristic diffraction peaks of SBA-15 disappeared, and a well-defined shoulder peak in range of 2Θ = 0.95-1.20° exhibited two diffraction peaks (211) and (220), showed the phase transformation from the 2d-hexagonal to the *Ia-3d* structure. After increasing amount of MPTMS high as 0.111 mol, the diffraction peak is broad exhibiting the low crystallinity of material results in the structure of material is collapsed to amorphous when amount of MPTMS to 0.179. The effect of MPTMS/(MPTMS+TEOS) ratio (4.1%-8.2%) on the phase transformation from high-curvature 2d-hexagonal to low-

curvature *Ia-3d*, showed **Figure 4.11**. can be explained that bounding of hydrophobic propyl thiol groups of MPTMS with hydrophobic PPO blocks than hydrophilic PEO blocks enlarges the hydrophobic volume and increases the hydrophobic/hydrophilic ratio [10]. If the hydrophobic/hydrophilic is less than 4.1%, the total of hydrophobic propyl thiol groups is not ample to remarkably enlarge the hydrophobic/hydrophilic ratio result in the cubic mesoporous does not obtain. Conversely, if it is increased higher than 10.2 %, the amorphous material is formed because co-condensation of silicon sources and structure directing agent will be disturbed [8]. Landry et. al. [6] explained phase transformation from hexagonal to cubic structure by longitudinal linkage of hexagonal pores "cylinder-merging" and transverse linkage "cylinder-branching" pathways. The phase transformation is depended on an increase in the value of the surfactant packing parameter $g = (V)/(a_0)(l)$, where V is the volume of hydrophobic chain, a_0 is area of hydrophilic part and l is length of hydrophobic chain. Increasing of g value affects to phase formation of hexagonal structure to cubic structure. The easy way to increase g is by connection of two cylinders of hexagonal phase, called cylinder merging. This mechanism can naturally propagate to form sheets of increasing width until another one was met by the assembly with a different orientation. The cylinder branching mechanism is based on structure fluctuations, forming of monkey saddle tower. Six neighboring cylinders around a central cylinder can be divided into 2 groups arranged symmetrically at (0°, 120°, 240°) and (60°, 180°, 300°). The central cylinder disrupted and served to connect the two groups of cylinders 3×3, lead to the two interleaved and connecting channels.

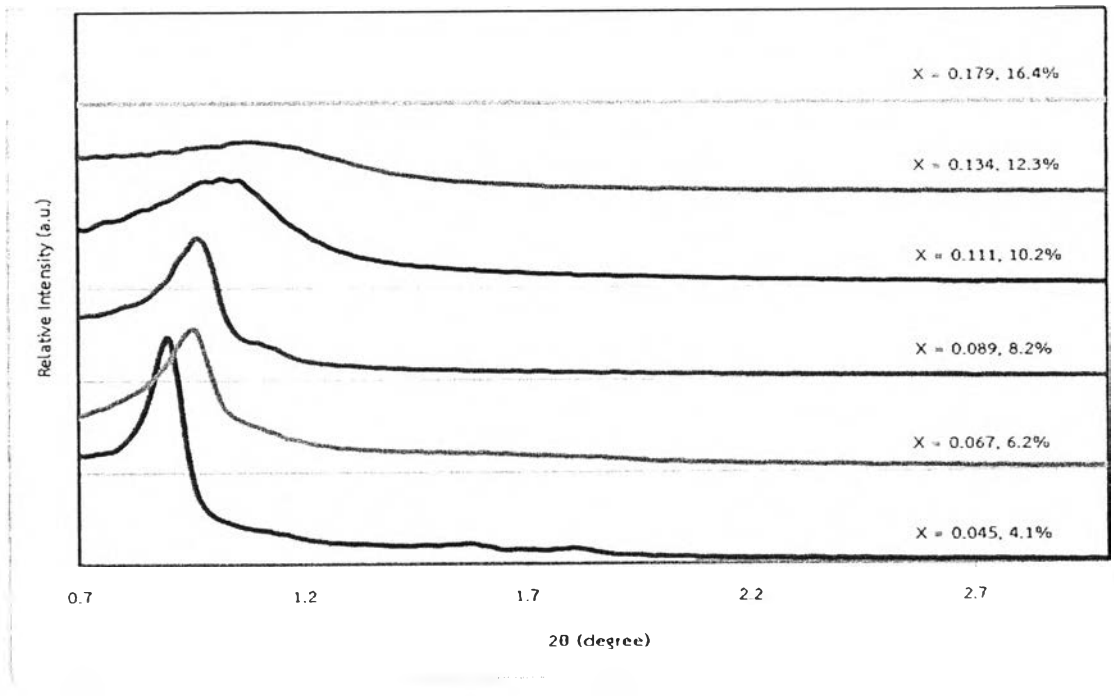

Figure 4.10 XRD patterns of MCAox with various the mol ratio of silicon source 1.089-*x* TEOS and *x* MPTMS by mole.

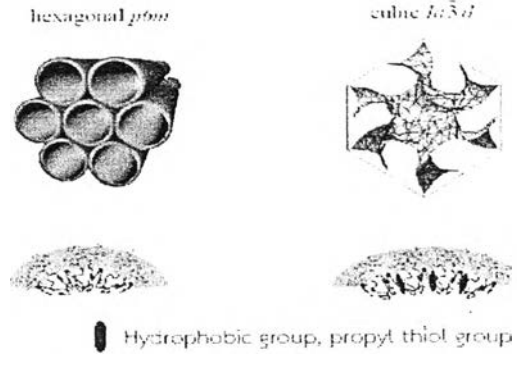

Figure 4.11 Phase transformation from from high-curvature 2d-hexagonal to low-curvature *Ia-3d* structure by adding MPTMS.

The SEM images showed the morphology of materials varied mole ratio of Si sources in **Figure 4.12 (a-f)**. At 0.045 mole of MPTMS, the morphology was an aggregated uniform particles with rope-liked form same with the hexagonal structure SBA-15 because high amount of TEOS covered the surfactant micelle that it very difficult for hydrophobic propyl thiol group to be formed with hydrophobic PO blocks. In range 0.067-0.111 mol of MPTMS, all materials exhibited rock-liked

morphology with proximate particle size. On the other hand, using 0.179 mol of MPTMS, the structure of material was distorted by the restraining self-crystallization of MPTMS to form silica particles. The amorphous materials was obtained because the self assembly between template and silicon sources will be disturbed

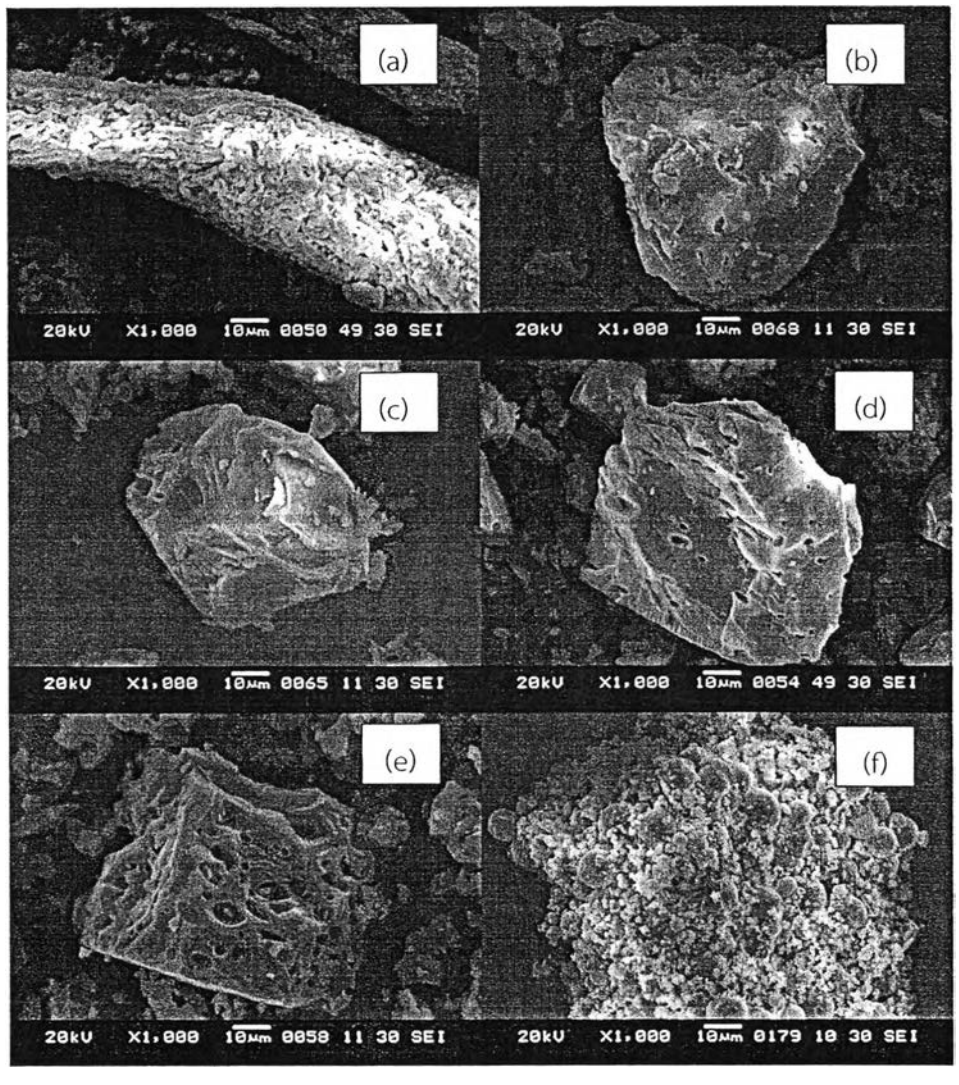

Figure 4.12 SEM images of MCAox synthesized by hydrothermal method with varied Si mole ratio 1.089-*x* TEOS : *x* MPTMS (a) *x*=0.045, (b) *x*=0.067, (c) *x*=0.089, (d) *x*=0.111, (E) *x*=0.134, and (f) *x*=0.179.

4.1.5 Effect of sequence of Si sources addition (TEOS and MPTMS)

In the synthesis of cubic *Ia-3d* mesoporous as opposed to total of MPTMS added, adding mixture of MPTMS and TEOS is important to obtain cubic *Ia-3d* structure. For the amount of MPTMS 8.2%, if pre-hydrolysis of MPTMS occurs prior to TEOS more than 15 min, the crystallinity of cubic structure materials is lower than

mixture of MPTMS and TEOS (**Figure 4.13a-c**). On the other side, if TEOS is pre-hydrolyzed before MPTMS addition within 15-30 min (**Figure 4.13d and e**), the lamella phase was obtained. The hydrolysis of TEOS prior to MPTMS added for 30 min or longer, the 2d-hexagonal SBA-15 is formed (**Figure 4.13f and g**). This phase transformation can be explained that if MPTMS and TEOS are mixed and then added to surfactant solution, the hydrophobic PO blocks will be bound to hydrophobic propyl thiol group of MPTMS causing the phase transformation from high-curvature 2d-hexagonal to low-curvature *Ia-3d* structure. When MPTMS was pre-hydrolyzed prior to TEOS adding within 15 to 60 min, the cubic structure is distorted having less structural orderness and tend to be amorphous material since the co-condensation of silicon sources and structure directing agent are disturbed. For adding TEOS prior to MPTMS 60 min or longer, the completing co-condensation of TEOS with structure directing agent before the hydrolysis of MPTMS with PPO blocks causes the 2d-hexagonal SBA-15 structure. Then the condition of synthesizing high ordered cubic *Ia-3d* by mixing of Si sources before added to surfactant solution will be used for the further study.

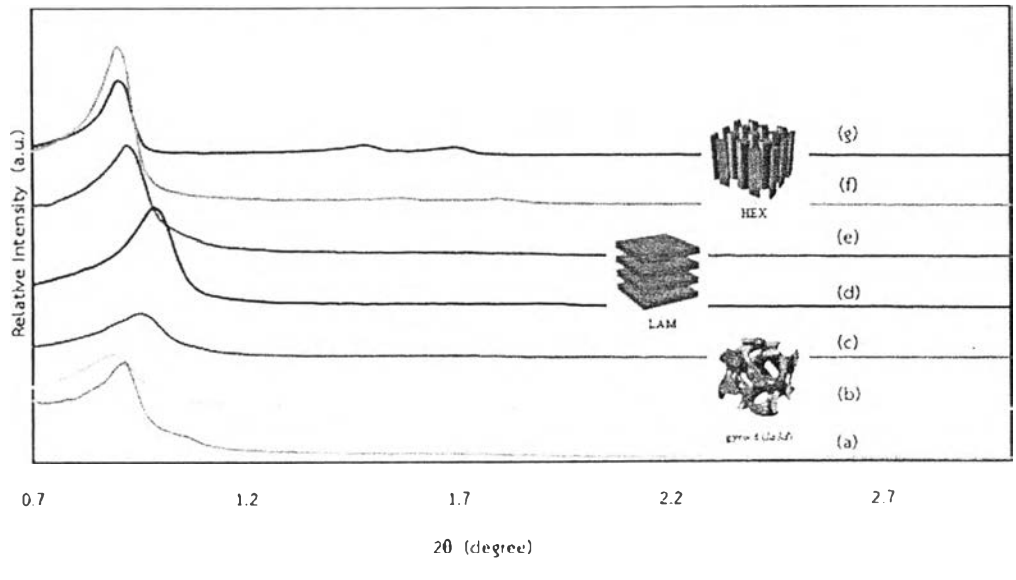

Figure 4.13 XRD Pattern of catalyst with varied sequence of input material by direct synthesis (a) MPTMS+TEOS 0 min, (b) MPTMS+TEOS 15 min, (c) MPTMS+TEOS 30 min, (d) TEOS+MPTMS 15 min, (e) TEOS+MPTMS 30 min, (f) TEOS+MPTMS 60 min and (g) TEOS+MPTMS 120 min.

4.1.6 The physico-chemical properties of sulfonic functionalized MCA synthesized by microwave method

4.1.6.1 XRD results

The XRD pattern of synthesized sulfonic cubic *Ia-3d* mesoporous silica by microwave method using aging time 1 hr. was showed in **Figure 4.14**. The gel composition was 1.0 TEOS: 0.089 MPTMS: 2.0 P123: 2.0 HCl: 148 H_2O which was similar with the optimum condition of synthesized by hydrothermal method. The XRD patterns showed a strong peak followed by a weak reflection at low-angle region 2θ 0.7- 3.0 degree which is mesostructured materials. The two peaks corresponds to (211) and (220) reflection of cubic *Ia-3d* mesostructure.

Comparison of extracted catalyst between hydrothermal and microwave method as shown in **Figure 4.15**, the crystallinity and shoulder peak height of lattice plane (220) of microwave catalyst was lower than hydrothermal method. The XRD pattern of microwave extracted catalyst was shifted to 2θ higher than hydrothermal catalyst showed the d-spacing and pore size distribution were lower. This can explain that the microwave radiation induced the condensation of silica and the dehydroxylation on the Si surface which leads to the formation of high crystalline pore wall [62].

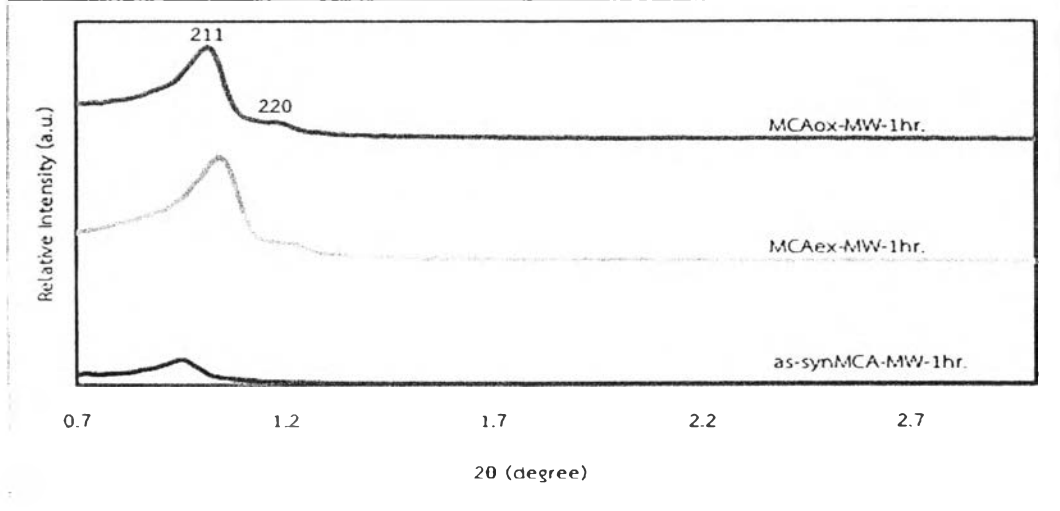

Figure 4.14 XRD patterns of XRD patterns of as-synthesized, extracted and oxidized MCA synthesized by microwave method using aging time 1 hr.

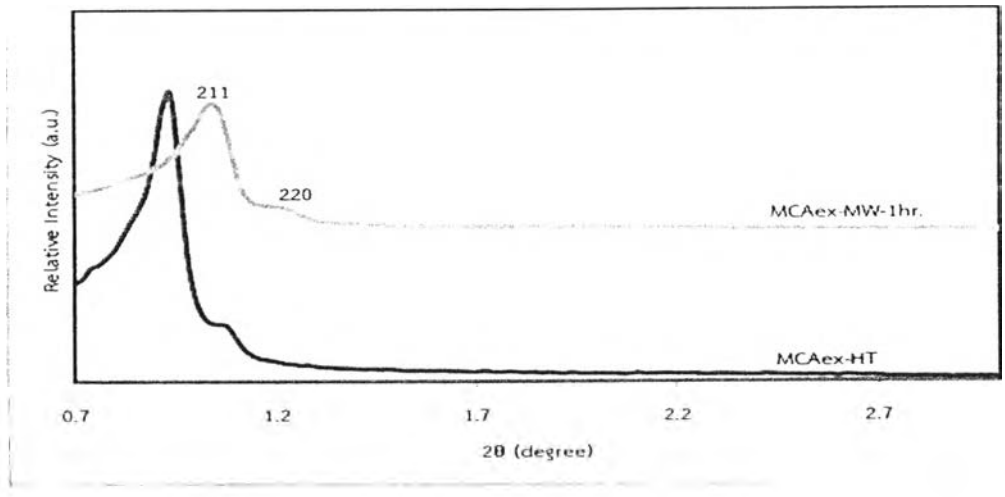

Figure 4.15 XRD patterns of comparison extracted catalyst between hydrothermal and microwave method.

4.1.6.2 Sorption properties

The N_2 adsorption-desorption isotherms of synthesized materials by microwave method showed the characteristic isotherm type IV which exhibited a well-defined H1 hysteresis loop according to the IUPAC classification relative to the mesoporous materials (shown in **Figure 4.16-4.17**). The hysteresis loop type H1 associated with pores consisting of agglomerates or compacts of uniform spherical particles with regular array, whose pore size distribution are normally narrow. The corresponding physical properties obtained from N_2 adsorption-desorption analysis are listed in **Table 4.2**. Removing structure directing agent from synthesized catalysts gives increasing of surface areas from 374.4 m^2/g to 544.3 m^2/g. However, the pore diameter of microwaved catalyst was lower than hydrothermal method, which conforming to XRD results. It may be caused from dehydroxylation on the Si by the microwave radiation [62].

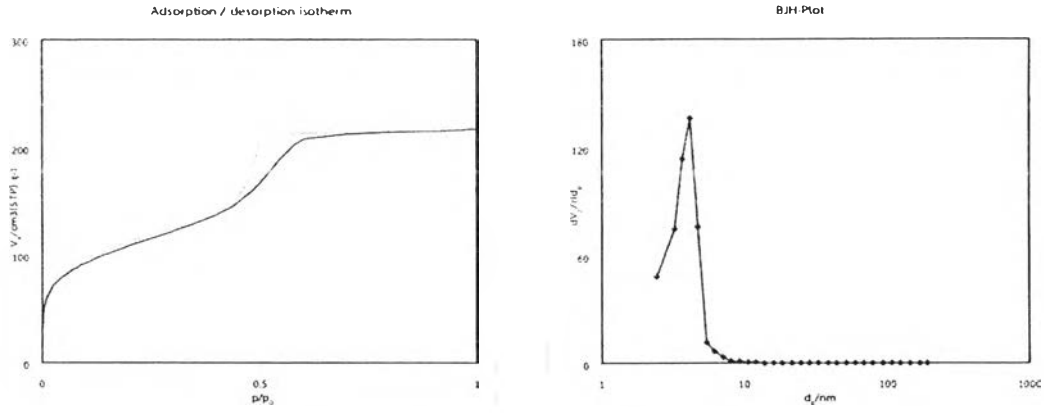

Figure 4.16 N_2 adsorption desorption isotherm and BJH-pore size distribution of MCAex synthesized by microwave method using aging time 1 hr.

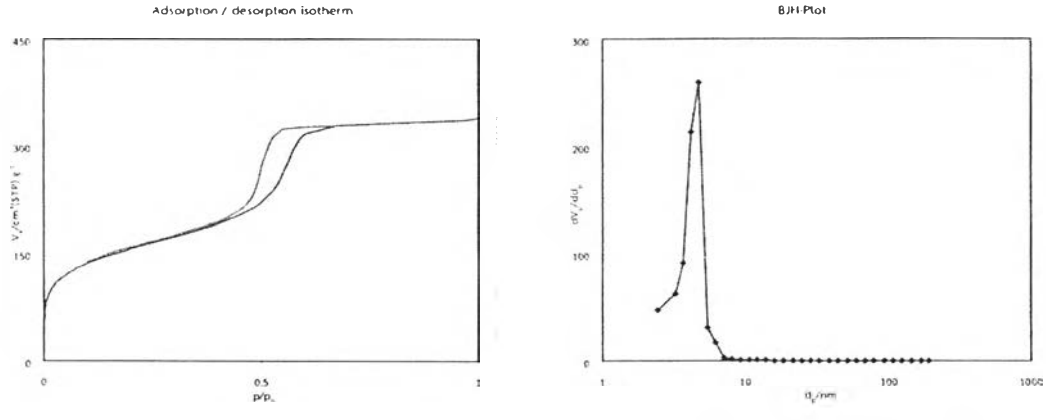

Figure 4.17 N_2 adsorption desorption isotherm and BJH-pore size distribution of MCAox synthesized by microwave method using aging time 3 hr.

Table 4.2 Textural properties of synthesized materials by microwave method.

Sample	S_{BET} $(m^2 g^{-1})^a$	Pore volume $(cm^3 g^{-1})^b$	Pore diameter $(nm)^b$	a_0 $(nm)^c$	Wall thickness $(nm)^d$
MCAex-MW-1hr.	374.4	0.3	4.2	20.8	10.5

Sample	S_{BET} ($m^2 g^{-1}$)[a]	Pore volume ($cm^3 g^{-1}$)[b]	Pore diameter (nm)[b]	a_0 (nm)[c]	Wall thickness (nm)[d]
MCAox-MW-1hr.	544.3	0.4	4.8	21.3	10.3

[a] BET specific surface area.

[b] Calculated by using the BJH method

[c] a_0 : cell parameter calculated from $a_o = \sqrt{6} \times d$ where d is d-spacing of the (211) reflection plane from XRD method

[d] wall thickness $T_{wall} = a_0 \sqrt{2}/2 - d_{pore}$, where d_{pore} and a_0 are pore distribution and cubic unit cell parameter respectively [58]

4.1.6.3 SEM images

The SEM images showed the morphology of MCAox synthesized by microwave method in **Figure 4.18**. The MCAox morphology was an aggregated particles form. In addition, the average particle size was in range 5-20 μm that was smaller than synthesized by hydrothermal method.

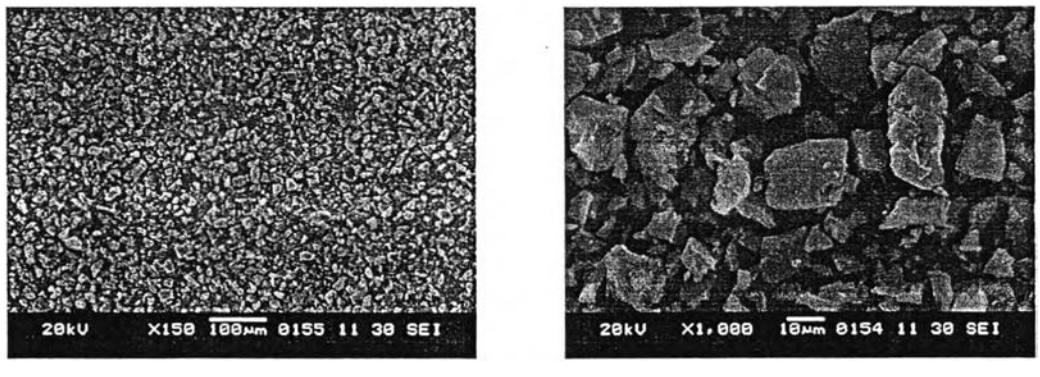

Figure 4.18 SEM images of oxidized MCAox synthesized by microwave method using aging time 1 hr.

4.1.6.4 TEM images

The TEM images cross section view of MCAox synthesized by microwave method were showed in **Figure 4.19**. It indicated the regular arrangement of mesochannels with pore size distribution 5.0-5.3 nm.

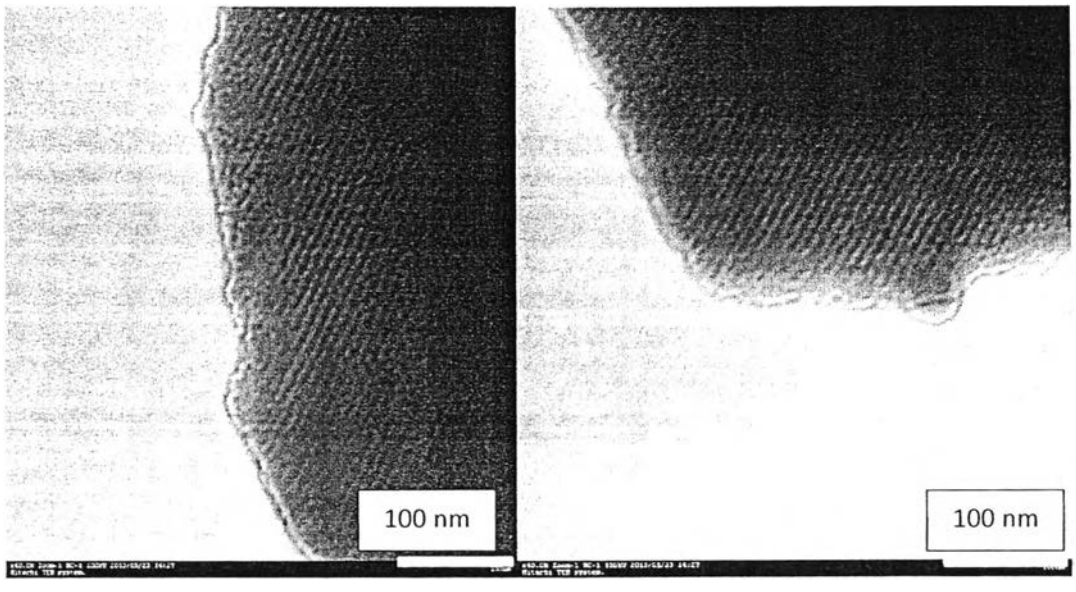

Figure 4.19 TEM images of MCAox synthesized by microwave method.

4.1.7 Effect of aging time by using microwave radiation

Synthesis cubic *Ia-3d* mesoporous silica using microwave method varied aging times from 0.5 to 4.0 hr. was characterized by X-ray diffraction technique. All materials exhibited the typical pattern of cubic *Ia-3d* mesostructure which had one very intense peak and one shoulder peaks indexed to (211) and (220) diffractions, respectively. Increasing the aging timeleads to higher crystallinity of materials. The surface properties of varied aging time catalysts were displayed in **Table 4.3**. Increasing aging times effected to raising pore diameter from 3.3 nm to 6.2 nm and specific surface area in range of 510.0–760.7 $m^2 g^{-1}$.

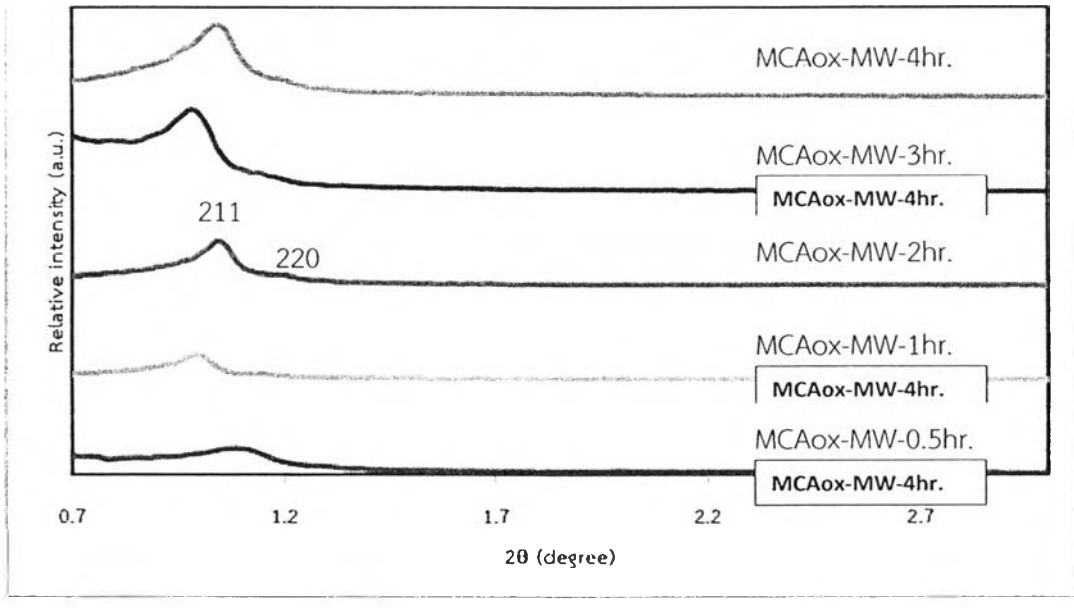

Figure 4.20 XRD patterns of synthesized materials by microwave method with varied aging temperature from 0.5-4.0 hr.

Table 4.3 Surface properties of microwave catalysts varied aging times.

Sample	S_{BET} ($m^2 g^{-1}$)[a]	Pore volume ($cm^3 g^{-1}$)[b]	Pore diameter (nm)[b]	a_0 (nm)[c]	Wall thickness (nm)[d]
MCAox-MW-0.5hr.	510.2	0.3	3.3	20.0	10.9
MCAox-MW-1hr.	544.3	0.4	4.8	21.3	10.3
MCAox-MW-2hr.	572.3	0.6	4.8	20.8	9.9
MCAox-MW-3hr.	621.6	0.5	5.4	20.8	9.3
MCAox-MW-4hr.	760.7	0.8	6.2	22.5	9.7

[a] BET specific surface area.

[b] Calculated by using the BJH method

[c] a_0 : cell parameter calculated from $a_o = \sqrt{6} \times d$ where d is d-spacing of the (211) reflection plane from XRD method

[d] wall thickness $T_{wall} = a_0 \sqrt{2}/2 - d_{pore}$, where d_{pore} and a_0 are pore distribution and cubic unit cell parameter respectively [58]

4.2 Post synthesis of hexagonal mesostructure SBA-15

4.2.1 The physico-chemical properties of SBA-15 materials

4.2.1.1 XRD results

Low angle X-ray powder diffraction patterns of as-synthesized SBA-15, SBA-15-Pr-SH and SBA-15-Pr-SO_3H were shown in **Figure 4.21**. The calcination to removal of triblock copolymer could improve intensity of peak. A very intense peak and two weak peaks indexed to (100), (110) and (200) diffractions that specified the prepared materials contained well-ordered hexagonal structure. The diffraction peaks of SBA-15-Pr-SO_3H were slightly shifted to higher 2 theta values when compared with SBA-15-Pr-SH, indicating pore size was decreased by bulky sulfonic group grafting on the surface of SBA-15-Pr-SH. This result was corresponding with surface analysis with N_2 adsorption desorption.

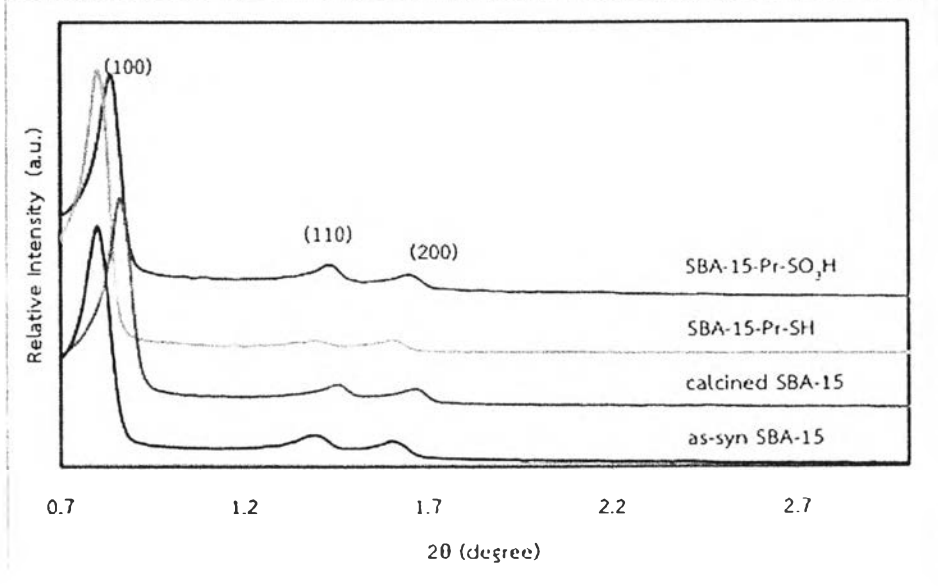

Figure 4.21 XRD patterns of synthesized SBA-15.

4.2.1.2 Sorption properties

The N_2 adsorption-desorption isotherm and pore size distribution of SBA-15 and functionalized SBA-15 were performed as a type IV of IUPAC classification and hysteresis loop was performed a H1-type, as shown in **Figure 4.22, 4.23**, that was a pattern of mesoporous materials. The physical properties calculated from the adsorption isotherm were filled in **Table 4.5**. The total specific surface areas of SBA-15 and SBA-15-Pr-SO_3H are 689.3 and 728.1 m^2/g, respectively. On the other hand, the pore size distribution of oxidized SBA-15 was lower than calcined SBA-15. This effect could explain that the organosulfonic acid group was functionalized into pore structure of SBA-15. These results were corresponded to XRD results.

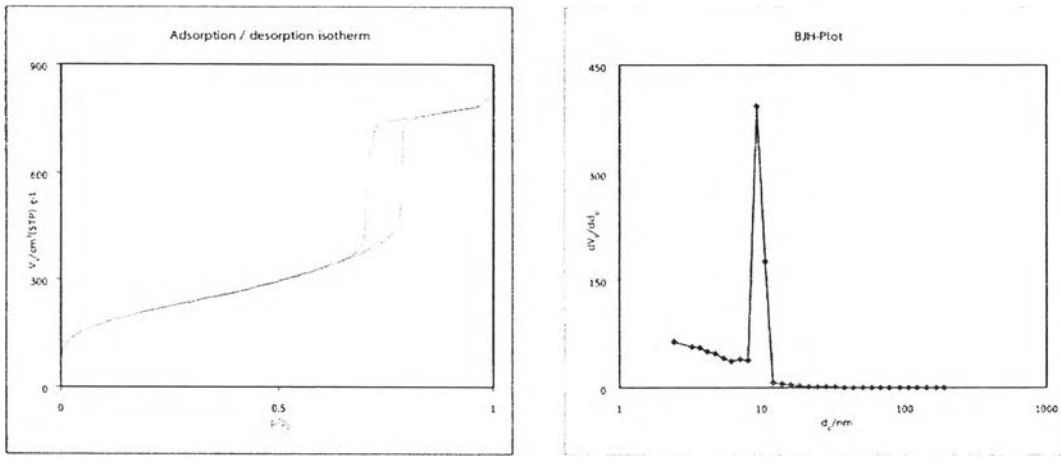

Figure 4.22 N_2 adsorption-desorption isotherm and BJH-pore sized distribution of SBA-15.

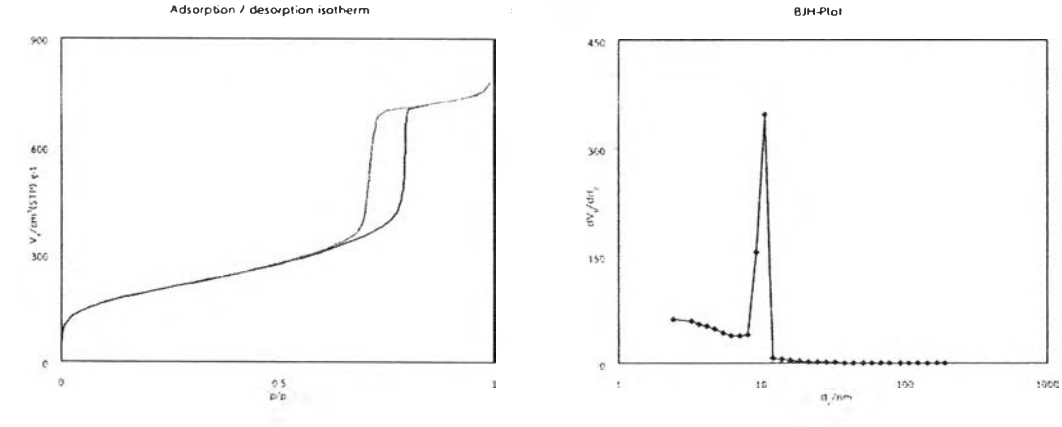

Figure 4.23 N_2 adsorption-desorption isotherm and BJH-pore sized distribution of SBA-15-Pr-SO_3H.

Table 4.4 Textural properties of SBA-15 and Sulfonic functionalized SBA-15.

Catalyst	S_{BET} $(m^2 g^{-1})^a$	Pore volume $(cm^3 g^{-1})^b$	Pore diameter $(nm)^b$	a_0 $(nm)^c$	Wall thickness $(nm)^d$
SBA-15	728.1	1.18	9.23	11.59	2.36
SBA-15-Pr-SO_3H	689.3	1.14	10.57	12.22	1.66

[a] BET specific surface area.

[b] Calculated by using the BJH method

[c] a_0 : cell parameter calculated from $a_0 = 2 \times d/\sqrt{3}$ where d is d-spacing of the (100) reflection plane from XRD method

[d] wall thickness calculated from $T_{wall} = a_0 - d_{pore}$, where d_{pore} and a_0 are pore distribution and hexagonal unit cell parameter respectively

4.2.1.3 SEM images

The SEM images of calcined and oxidized SBA-15 are illustrated in Figure 4.22. Morphology of SBA-15 was uniform rope-like particle shape aggregated particles. In addition, the size of calcined SBA-15 particles was smaller than oxidized SBA-15. This observation was assumed that coating propyl sulfonic group on the surface of materials led to increasing of pore volume which affecting on particle shapes.

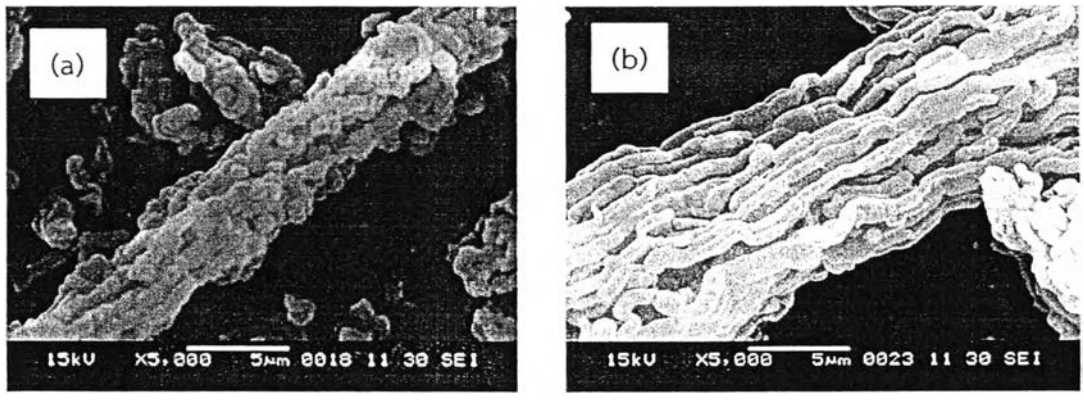

Figure 4.24 SEM images of (a) SBA-15 and (d) SBA-15-Pr-SO_3H.

4.3 Acidity from titration and pore size distribution of catalysts

The acidity of synthesized material was measured quantitatively by acid-base titration using sodium chloride as ion exchange agent. In this work, both of synthesized catalysts by hydrothermal and microwave methods with same gel composition gave no significantly differential acid values (**Table 4.5**). The commercial catalyst Amberlyst-15 shows the highest acidity. Pore size distribution of zeolite such as Beta, ZSM-5 and MCM-22 is lower than 0.8 nm which lower than synthesized catalyst because it is microporous material.

Table 4.5 The acid value and pore size of catalysts.

Catalyst	Acidity (mmol/g)	Pore size (nm)
Amberlyst-15	4.0	26.0
Acidic clay	2.0	-
Direct-SBA-15-Pr-SO_3H	1.5	6.6
Post-SBA-15-Pr-SO_3H	1.4	9.2
MCAox-HT	1.4	5.4
MCAox-MW-1hr	1.2	4.8
FSM-16-Pr-SO_3H	1.1	2.4
MCM-22	0.8	0.5
MCAex-HT	0.7	5.4
Beta	0.7	0.8
ZSM-5	0.5	0.5
Nafion SAC-13	0.2	>10.0

4.4 Acidity from NH_3-TPD

From NH_3-TPD experiment, total amount of ammonia desorbed was related to the number of acid site whereas the maximum temperature of desorption provided an indication of acid strength. The NH_3-TPD profiles of both samples were shown in **Figure 4.25** and list of acidic properties was shown in **Table 4.6**. The NH_3-TPD profile of Amberlyst-15 shows broad peak at 511-568°C, which correspond to desorption of the NH_3 on strong acidic site. Acidic amount of Amberlyst-15 is lower than synthesized catalyst because of decomposed structure by high temperature. Both of oxidized catalysts from hydrothermal and microwave showed 2 peaks region at 150-250°C, corresponding to weak acid site, and 500-600°C which indicating to strong acid site.

1. Amberlyst-15

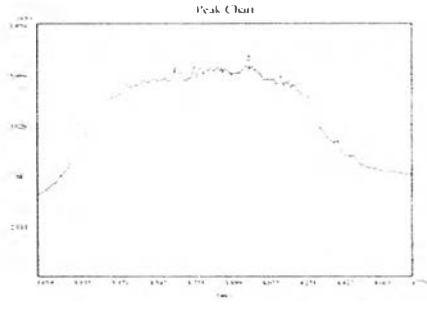

2. MCAox-MW

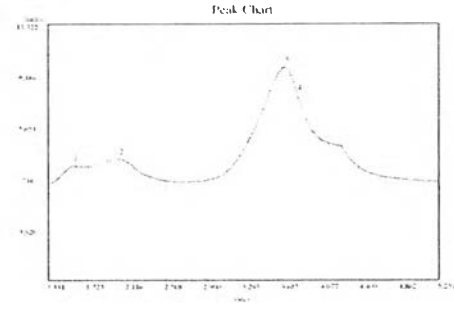

3. MCAox-HT

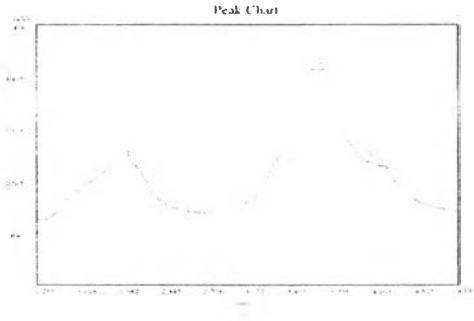

Figure 4.25 NH_3-TPD profile profiles of synthesized catalyst and commercial catalyst.

Table 4.6 Acidic properties of catalysts measured by NH_3-TPD.

Catalysts	peaks	peak position (°C)	mmol	mmol/g	Total (mmol/g)	Acid from titrate (mmol/g)
Amberlyst-15	1	511.0	0.049	0.569	1.781	4.0
	2	568.0	0.103	1.212		
MCAox-MW	1	163.0	0.007	0.084	2.764	1.2
	2	244.0	0.033	0.418		
	3	518.0	0.110	1.381		
	4	540.0	0.070	0.881		
MCAox-HT	1	241.0	0.057	0.716	2.737	1.4
	2	517.0	0.131	1.636		
	3	585.0	0.031	0.385		

4.5 Thermal gravimetric Analysis (TGA)

Thermal stability test of catalysts combining thermal gravimetry (TGA) and differential thermal analysis (DTA) was measured by Metler Toledo TGA/SDTA 851 at a heating rate of 10°C/min in nitrogen from 30°C to 1,000°C. The thermal stability of MCAox-HT (MCA-Pr-SO_3H) and Post-SBA-15-Pr-SO_3H were showed in **Figure 4.26 and 4.27**. MCAox-HT and SBA-15-Pr-SO_3H exhibited a weight loss below 100 °C, 13.1% and 11.9%, respectively. It indicated to lose of water in pore of catalyst. Moreover, at temperature region from 230°C to 615°C of MCAox-HT and 210°C to 620°C of SBA-15-Pr-SO_3H with weight losing 8.4% and 10.7% indicated the decomposition of the sulfonic group [63].

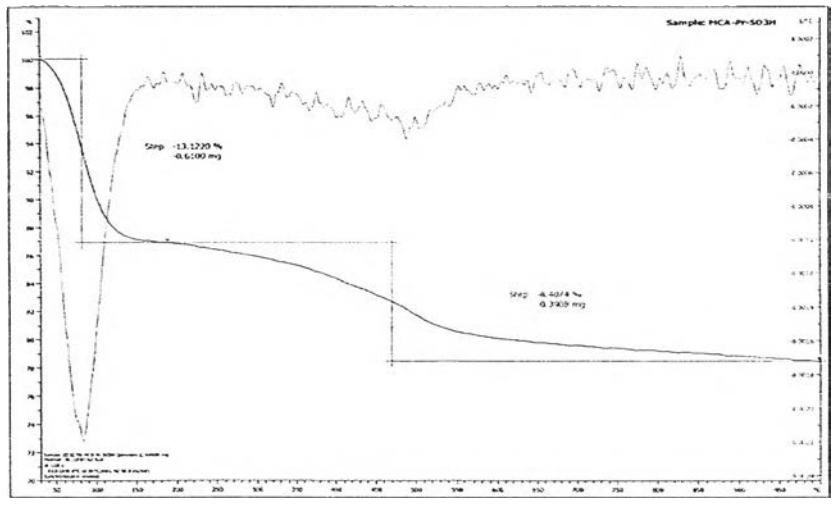

Figure 4.26 Thermal gravimetric profile of MCAox-HT.

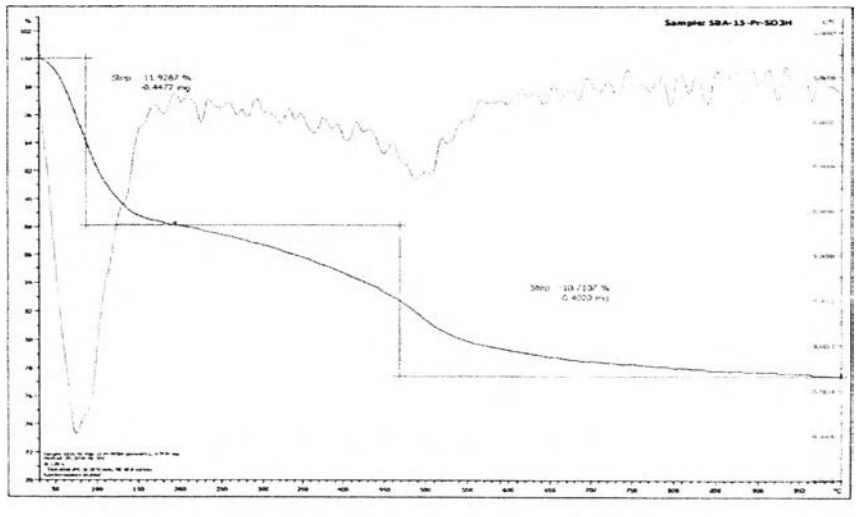

Figure 4.27 Thermal gravimetric profile of Post-SBA-15-Pr-SO_3H.

The thermal gravimetric of Amberlyst-15 profile was shown in **Figure 4.26**. Its weight lost in 3 steps, at 100°C, 20.3% losing weight due to removal of absorbed water. At 240°C-630°C, 2 step losing weights about 21.9% and 27.7% owing to decomposition of sulfonic group and polymeric resin, respectively [64].

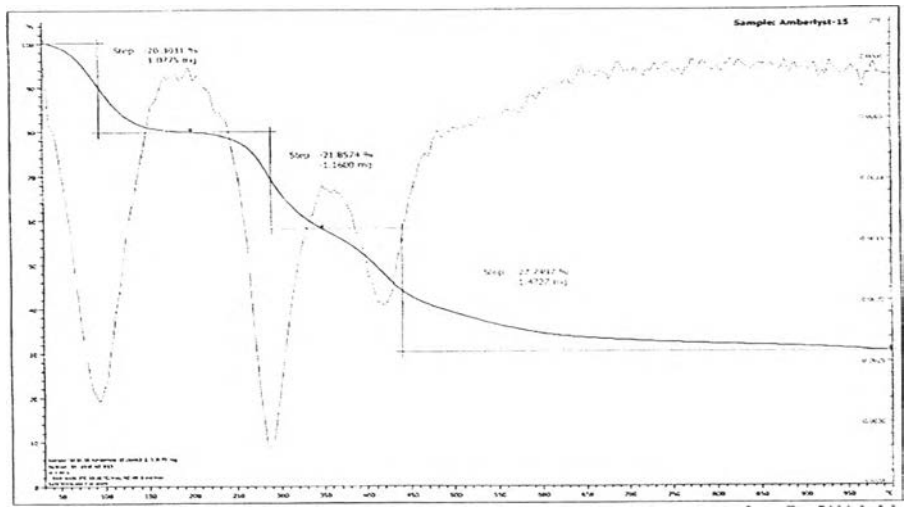

Figure 4.28 Thermal gravimetric profile of Amberlyst-15.

Table 4.7 found that post-SBA-15-Pr-SO3H, MCAox and Amberlyst-15 have similarly stability but cubic *Ia-3d* mesoporous silica, MCAox, was more stable than other catalysts because it was less loser propyl sulfonic group than Amberlyst-15 and post-SBA-15-Pr-SO_3H at high temperature.

Table 4.7 Comparison of catalyst stability.

Catalysts	Temperature (°C)	Weight lost of catalyst (%weight)
Post-SBA-15-Pr-SO_3H	0-100	11.9
	210-620	10.7
MCA-Pr-SO_3H, MCAox	0-100	13.1
	230-615	8.4
Amberlyst-15	0-100	20.3
	240-630	21.9 and 27.7

4.6 Catalytic activity of Amberlyst-15 in esterification of glycerol with acetic acid

Esterification of glycerol with acetic acid using Amberlyst-15, commercial catalyst, was studied to find an optimum condition of triacetin synthesis. The optimum reaction condition over Amberlyst-15 for triacetin synthesis was

investigated with various reaction parameters, *i.e.* reaction temperature, mole ratio of reactants, catalytic amount and reaction time.

4.6.1 Effect of reaction times

Impact of reaction time on product yield and selectivity achieved from esterification of glycerol with acetic acid, using a commercial catalyst called Amberlyst-15 is shown in **Table 4.8**. The yield of triacetin was calculated by calibration curve formula $y = 0.3729x + 0.17$ with $R^2 = 0.9949$ where y and x are weight and area ratio of triacetin to internal standard, respectively. It can be seen that Amberlyst-15 gives high glycerol conversion after 0.5 h (92.9%), indicating a high activity of catalytic resin. At reaction time of 1.0 hr., the highest yield of triacetin (14.6%) is observed. Upon increasing reaction time beyond 1.5 hr., selectivity of 1,2 diacetin formation increases due to reversibility of esterification reaction. Moreover, products from esterification can be changed into other forms by acetylation with acetic acid or deacetylation, reacted with water as nucleophile.

Table 4.8 Effect of reaction time on product yields and selectivity over Amberlyst-15.

Reaction time (hr.)	% conversion	% yield triacetin	Selectivity (%)				
			Tri	1-mono	2-mono	1,3-di	1,2-di
0.5	92.9	10.2	18.3	4.4	26.8	21.2	29.3
1.0	95.9	14.6	10.7	3.6	32.5	14.7	38.5
1.5	98.6	14.1	11.3	3.3	29.7	14.4	41.3
2.0	97.2	13.9	11.5	3.2	29.4	14.4	41.5

Reaction conditions: glycerol:acetic acid as 1:6 by mole, 4 wt% of Amberlyst-15 based on weight of reaction mixture and temperature = 115°C

4.6.2 Effect of catalytic amount

Results in **Table 4.9** indicated influences of amount of catalyst on conversion and product selectivity. Increasing amount of catalyst from 0 to 8 wt.% could enhance glycerol conversion. Glycerol can be converted to acetylated products under this condition without catalyst but the main product was 2-monoacetin. This result showed that acid catalyst was important to induce esterification reaction.

Catalyst loading of 4 wt.% based on weight of reaction mixture gave the highest yield of triacetin (14.6%).

Table 4.9 Effect of catalyst amount on product yields and selectivity over Amberlyst-15.

Catalytic amount (wt.%)	% conversion	% yield triacetin	Selectivity (%)				
			Tri	1-mono	2-mono	1,3-di	1,2-di
0	80.9	0.0	0.0	8.4	71.6	5.3	14.7
2	97.1	11.2	3.6	15.6	31.1	11.4	38.3
4	95.9	14.6	10.7	3.6	32.5	14.7	38.5
6	97.5	11.2	11.4	3.4	30.8	14.8	39.6
8	97.7	11.5	12.9	3.5	30.5	15.7	37.4

Reaction conditions: glycerol:acetic acid as 1:6 by mole, reaction time = 1 hr. and temperature = 115°C

4.6.3 Effect of glycerol to acetic acid mole ratio

Influence of glycerol to acetic acid mole ratio on conversion and product selectivity was summarized in **Table 4.10**. Results indicated that an increase amount of acetic acid in a mixture from 1:3 to 1:24 by mole led to a raise of aspiring product. Nevertheless, further increment in mole ratio beyond 1:15 showed insignificant increase in %yield of triacetin. This result suggested that glycerol to acetic acid mole ratio of 1:15 was an optimum for reaction temperature testing.

Table 4.10 Effect of mole ratio on product yields and selectivity over Amberlyst-15.

glycerol : acetic acid mole ratio	% conversion	% yield triacetin	Selectivity (%)				
			Tri	1-mono	2-mono	1,3-di	1,2-di
1:3	92.9	4.9	5.3	6.7	48.5	13.4	26.1
1:6	95.9	14.6	10.7	3.6	32.5	14.7	38.5
1:9	98.6	19.4	19.7	2.3	21.1	14.7	42.2

glycerol : acetic acid mole ratio	% conversion	% yield triacetin	Selectivity (%)				
			Tri	1-mono	2-mono	1,3-di	1,2-di
1:12	99.5	22.2	25.2	1.8	16.1	16.0	40.9
1:15	99.4	30.2	26.9	1.6	14.2	16.6	40.7
1:18	99.6	31.5	30.7	1.4	12.0	16.3	39.6
1:21	99.7	34.9	33.2	1.2	10.9	15.6	39.1
1:24	99.9	34.2	33.2	1.1	9.9	15.8	40.0

Reaction conditions: 4 wt% of Amberlyst-15 based on weight of reaction mixture, reaction time = 1 hr. and temperature = 115°C

4.6.4 Effect of reaction temperature

Effect of reaction temperature was shown in **Table 4.11**. The glycerol was increasingly converted to triacetin as reaction temperature was raised from 95°C to 105°C. Nevertheless, at 115°C results showed high glycerol conversion but reduction in %yield of triacetin was observed because acidity of Amberlyst-15 was lost at high temperature due to the limitation of operating temperature at 120°C [65]. Moreover, this observation may be attributed to side reaction of glycerol shown in **Scheme 4.1**. The formation of α-hydroxyacetone (acetal) from dehydration of glycerol can be observed for all catalytic studies. Furthermore, acrolein can be observed by dehydration at a central hydroxyl group, shown in **Scheme 4.2** [13]. However, peaks of acetal and acrolein, which have a lower boiling point than acetylated products, was indiscernible because they were included with the solvent peak in this GC analysis conditions. Increasing time with various temperature reactions showed higher yield of triacetin both at 95°C and 105°C. As expected, changes in glycerol conversion were not significant both 95°C and 115°C. At 105°C, reaction time of 1 hr. gave higher selectivity and %yield of triacetin than 3 hr. This effect may be caused by deacetylation. A result showed that %yield of triacetin was enhanced by increasing the reaction temperature to 105°C as well as increasing reaction time.

Table 4.11 Effect of temperature and time on product yields and selectivity over Amberlyst-15.

Temp. (°C)	Time (hr.)	% conversion	% yield triacetin	Selectivity (%)				
				Tri	1-mono	2-mono	1,3-di	1,2-di
95	1.0	99.7	20.6	26.1	1.5	14.0	16.4	42.0
95	3.0	99.6	23.7	22.1	14.2	12.8	14.4	36.5
105	1.0	99.4	33.7	33.9	1.6	13.4	16.1	35.0
105	3.0	99.7	36.5	28.3	2.0	15.2	19.1	35.4
115	1.0	99.4	30.2	26.9	1.6	14.2	16.6	40.7

Reaction conditions: glycerol:acetic acid as 1:15 by mole, 4 wt% of Amberlyst-15 based on weight of reaction mixture

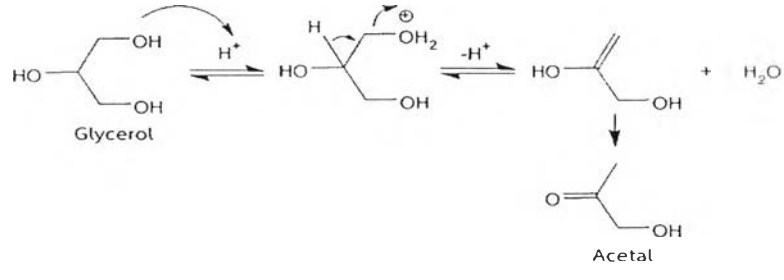

Scheme 4.1 Mechanism of acetal formation by acid catalysts.

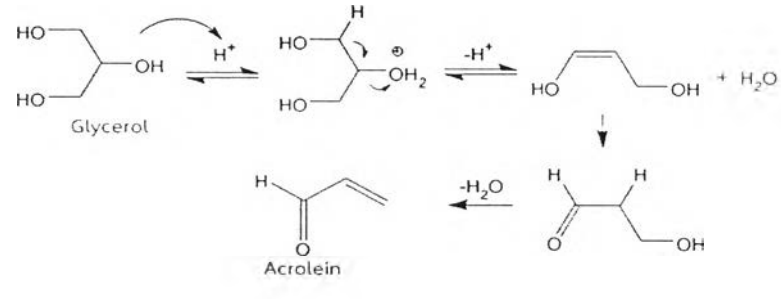

Scheme 4.2 Mechanism of acrolein formation by acid catalysts.

4.7 Catalytic activity of cubic *Ia-3d* mesoporous silica in esterification of glycerol with acetic acid

The optimum condition to synthesize triacetin using Amberlyst-15 was glycerol to acetic acid 1:15 by mole, reaction temperature 105°C, catalytic amount 4 wt% at reaction time 1 hr., shown in **Table 4.11**. We used this condition to test efficiency of synthesized catalyst which was compared with other catalysts such as zeolite, mesoporous material and commercial catalysts. This result showed that acid site was important to induce esterification reaction. The influence of temperatures at 105°C and 115°C were studied. Generally, 99% conversion of glycerol is achieved within 1 hr. However, with the usage of MCM-22, the % conversion is lowered due to inappropriate small pore structure to this glycerol esterification. At reaction temperature 105°C, Amberlyst-15 gave the highest selectivity to triacetin (33.9%) but it was decreased when increasing temperature to 115°C. The above phenomenon shows that the Amberlyst-15 may break up because it is close to its limited temperature (120°C) [65]. Although, Amberlyst-15, commercial catalyst, has a great acidity (4.0 mmol/g in **Table 4.5**) over other synthesized catalysts but surface area is lower than the synthesized catalyst (53 m^2/g). It can be indicated that the number of active site of Amberlyst-15 is less but strong acid site. Because of the temperature restriction of Amberlyst-15 (120°C), the milder reaction temperature (105°C) with higher mole ratio of acetic acid to glycerol is the best alternative to increase the substituted acetylated derivatives (triacetin) [14].

For small pore of zeolite catalysts, ZSM-5 and MCM-22, is more selected to 2-monoacetin and shows a lower glycerol conversion than others maybe the diameter of reactant and products, shown in **Table 4.14**, are larger than their pore size of the zeolites, 0.5 nm (**Table. 4.5**). The pore size of zeolite beta is 0.8 nm which prefer to formation of diacetin at 150°C. In addition, increasing reaction temperature to 115°C can raise selectivity of triacetin, The ion-exchange resin is more active than zeolite because of their higher number of acidic active site and configurational diffusion effect [14]. From the results at 105°C, the selectivity of triacetin is about 27.5% and increased by raising temperature (115°C) to 38.2% when using MCA-Pr-SO_3H-MW-1H. This effect may occur from the synthesized catalysts were not successfully activated and this influence can be seen with MCA-Pr-SO_3H-HT. The high selectivity of triacetin from both hydrothermal and microwave method was insignificant, 39.6% and 38.2%, respectively, because of high surface areas and three-dimensional channels which the opportunity reacting is higher than the 2d-hexagonal structure SBA-15.

Table 4.12 Esterification of acetic acid with different catalysts at 105°C.

Catalyst	% Glycerol conversion	% yield triacetin	% Selectivity				
			tri	1-mono	2-mono	1,3-di	1,2-di
Amberlyst-15	99.4	33.7	33.9	1.6	13.4	16.1	35.0
SBA-15-Pr-SO_3H	99.6	26.0	25.7	1.3	12.6	15.4	45.0
MCA-Pr-SO_3H-MW 3H	100.0	23.3	27.5	1.7	13.9	16.9	40.0
FSM-16-Pr-SO_3H	99.7	16.7	23.4	1.7	16.2	15.5	43.2
clay	99.8	14.6	15.0	1.7	15.7	19.2	48.4
Direct SBA-15-Pr-SO_3H	99.3	14.1	27.2	1.7	14.2	17.2	39.7
MCA-Pr-SO_3H- HT	100.0	9.2	13.7	2.1	19.5	17.0	47.7
Nafion SAC-13	99.2	12.7	10.0	2.8	24.7	17.7	44.8
Beta	98.6	0.0	0.0	4.4	35.0	15.7	44.9
ZSM-5	79.6	0.0	0.0	15.4	69.9	5.3	9.4
MCM-22	59.8	0.0	0.0	7.7	69.8	5.8	16.7

Reaction conditions: glycerol:acetic acid as 1:15 by mole, 4 wt% of catalyst based on weight of reaction mixture, T = 105°C, t = 1 hr.

Table 4.13 Esterification of acetic acid with different catalysts at 115°C.

Catalyst	% Glycerol conversion	% yield triacetin	% Selectivity				
			tri	1-mono	2-mono	1,3-di	1,2-di
MW-MCAox-3H	99.8	33.5	38.2	1.1	9.6	14.9	36.2
HT-MCA-Pr-SO_3H	99.7	30.1	39.6	2.2	10.9	24.1	23.2
Amberlyst-15	99.4	30.2	26.9	1.6	14.2	16.6	40.7
Nafion SAC-13	99.6	29.5	18.2	1.9	17.1	18.6	44.2
SBA-15-Pr-SO_3H	99.9	25.6	38.4	1.7	12.6	18.8	28.5
Acidic clay	99.7	22.5	27.2	1.3	17.8	13.5	40.2
FSM-16-Pr-SO_3H	99.5	20.7	35.9	2.7	12.9	23.4	25.1
Direct SBA-15-Pr-SO_3H	99.3	16.9	32.0	1.41	12.65	15.9	38.3
Beta	99.3	16.2	15.7	2.9	11.3	36.0	34.1
ZSM-5	94.9	12.6	1.1	8.5	39.9	21.4	29.1
MCM-22	76.8	0.0	0.0	7.2	62.0	8.8	22.0

Reaction conditions: glycerol:acetic acid as 1:15 by mole, 4 wt% of catalyst based on weight of reaction mixture, T = 115°C, t = 1 hr. with SD within ± 0.02

Table 4.14 Size of acylated products structure estimated from Hyper-chem program.

Products	Size of structures	
	Width (nm)	Long (nm)
Triacetin	0.85	0.99
1,3-diacetin	0.40	0.99
1,2-diacetin	0.68	0.78
1-monoacetin	0.41	0.79
2-monoacetin	0.58	0.59
glycerol	0.25	0.48
Acetic acid	0.13	0.28

4.8 Esterification of glycerol with long chain carboxylic acid

Table 4.15, 4.16 and 4.17 showed the reactivity of different carboxylic acids caproic acid (C_6), lauric acid (C_{12}) and oleic acid (C_{18}) for glycerol esterification at 110°C with various reaction times which catalyzed by sulfonic cubic *Ia-3d* mesoporous silica, Amberlyst-15 and 2d-hexagonal direct SBA-15-Pr-SO_3H, respectively. An increasing 99% of the glycerol conversion was achieved within 0.5 hr. by using MCAox at 110°C. However, it took 1 hr. for esterification to reach the same level of conversion when catalyzed by Amberlyst-15 in cases of caproic acid and lauric acid. These results suggested the MCA mesoporous catalyst in catalyzing this reaction could perform faster than resin catalyst. Using increased reaction times will raise the selectivity of triglyceride. Although the glycerol transforms completely at an immediate time, the selectivity of triglyceride was increased by esterification of fatty acids to monoglycerides and diglycerides. These results can be proven by the decrease in selectivity of monoglyceride and diglyceride. The esterification can be reversed by promotion of water, a by-product from the reaction. Moreover, it can preserve the catalytic activity by nitrogen gas flowing in order to remove water from the reaction and to provide an inert atmosphere.

Both of synthesized sulfonic MCA catalysts from hydrothermal and microwave methods give higher selectivity to triglyceride than Amberlyst-15 and SBA-15-Pr-SO_3H

at the similar condition. For caproic acid reaction, the MCAox gave high efficient selectivity of triglyceride about 96% while Amberlyst-15 and SBA-15-Pr-SO_3H were 93% and 64% at 4 hr. Increasing hydrophobic carbon chains to lauric acid and oleic acid, all catalysts still gave a high glycerol conversion meanwhile less selective triglyceride was obtained. Synthesized catalyst from microwave method is lower catalytic efficiency than hydrothermal method because of the lower pore size 4.8 nm that show clearly effect with large free fatty acid molecules. Compare with 2d-hexagonal structure SBA-15-Pr-SO_3H by direct synthesis, cubic *Ia-3d* mesoporous silica showed higher efficiency selective to triglyceride at similar condition although it was higher in acidity and pore size. Because multi dimensional pore channel causes the reactant easily pass through inside of catalyst.

The diminishing trend in carboxylic acid reactivity with raising alkyl chain length C_6 to C_{18} by using acid catalysts can be explained by two components inductive effect and steric effect [66]. The inductive effect was occurred by increasing in electron-releasing ability of the acid with lengthening alkyl chain. Even if the protonation of the carbonyl carbon was simplified by the inductive effect, it reduces the electrophilicity of the carbonyl carbon. Thus, an energy-hindered rate-limiting nucleophilic attack of hydroxyl of glycerol is more. The steric component is the important factor for acid-catalyzed esterification [66-68]. The carbon chain length increased with steric hindrance that causing electronic repulsion between nonbonding atoms of reacting molecules. An electron density in the intermolecular region is decreased and bonding interaction is disturbed by this repulsive hindrance [67] that can support our observation.

Table 4.15 Esterification of glycerol with caproic acid.

Catalyst	Reaction time (hr.)	%Glycerol conversion	%Selectivity				
			tri	1-mono	2-mono	1,3 di	1,2 di
Amberlyst-15	0.5	81.4	0.0	65.1	23.5	3.1	8.3
	1	98.3	6.7	2.5	20.0	21.6	49.1
	2	100.0	50.6	0.3	2.0	13.1	34.0
	3	99.3	87.0	0.0	0.0	4.2	8.8
	4	100.0	93.4	0.0	0.0	2.0	4.6
MCAox-HT	0.5	100.0	16.0	1.5	14.7	21.8	46.0
	1	100.0	40.5	0.3	3.6	16.8	38.7
	2	100.0	72.0	0.0	0.5	7.3	20.2
	3	100.0	86.5	0.0	0.1	4.2	9.2
	4	100.0	96.0	0.1	0.1	1.0	2.8
MCAox-MW	0.5	98.7	32.4	0.0	0.0	12.6	55.0
	1	99.5	53.7	0.0	0.0	9.8	36.5
	2	100.0	88.4	0.0	0.0	1.5	10.1
	3	100.0	92.7	0.0	0.0	1.4	5.9
	4	100.0	96.2	0.0	0.0	0.8	3.0
Direct SBA-15-Pr-SO_3H	0.5	96.9	5.5	5.0	42.8	17.2	29.6
	1	97.7	12.6	3.2	27.7	21.6	34.9
	2	98.7	27.6	1.9	16.8	21.8	31.9
	3	99.2	45.9	2.2	16.6	15.3	20.1
	4	99.8	63.8	1.6	11.2	9.8	13.6

Reaction Condition: glycerol:captroic acid mole ratio 1:6, T = 110°C, catalyst 5% base on total reaction mixture

Table 4.16 Esterification of glycerol with lauric acid.

Catalyst	Reaction time (hr.)	%Glycerol conversion	%Selectivity				
			tri	1-mono	2-mono	1-3 di	1-2 di
Amberlyst-15	0.5	81.4	0.0	65.1	23.5	3.1	8.3
	1	98.3	6.7	2.5	20.0	21.6	49.1
	2	100.0	50.6	0.3	2.0	13.1	34.0
	3	99.3	87.0	0.0	0.0	4.2	8.8
	4	100.0	93.4	0.0	0.0	2.0	4.6
MCAox-HT	0.5	99.3	27.8	1.9	4.3	27.4	38.6
	1.0	100.0	73.5	0.0	0.0	8.1	18.4
	2.0	100.0	82.7	0.2	0.5	6.6	10.0
	3.0	100.0	93.3	0.0	0.0	2.9	3.8
	4.0	100.0	96.4	0.0	0.0	1.4	2.2
MCAox-MW	0.5	99.9	10.6	8.4	15.1	20.5	45.5
	1	100.0	35.8	1.4	0.8	16.4	45.5
	2	100.0	59.8	0.5	0.2	8.8	30.7
	3	100.0	68.3	0.4	0.3	7.8	23.3
	4	100.0	82.2	0.0	0.0	2.8	15.0
Direct SBA-15-Pr-SO_3H	0.5	84.3	0.0	21.3	36.5	10.3	31.9
	1	94.3	2.5	13.7	38.6	19.4	25.8
	2	100.0	14.8	4.0	1.2	29.4	50.6
	3	100.0	32.2	0.0	0.0	13.1	54.7
	4	100.0	79.6	0.0	0.0	0.0	20.4

Reaction Condition: glycerol :lauric acid mole ratio 1:6, T = 110°C, catalyst 5% base on total reaction mixture

Table 4.17 Esterification of glycerol with oleic acid

Catalyst	Reaction time (hr.)	%glycerol conversion	%selectivity				
			tri	1-mono	2-mono	1-3 di	1-2 di
Amberlyst-15	0.5	88.4	0.0	9.8	90.2	0.0	0.0
	1	87.6	0.0	9.8	86.0	1.4	2.8
	2	87.9	0.0	19.1	71.9	4.0	5.0
	3	86.6	0.0	9.5	77.0	5.1	8.4
	4	98.7	3.1	3.6	33.1	18.0	42.2
	5	99.7	15.3	1.4	13.8	20.9	48.6
	6	99.9	41.3	1.5	7.0	17.3	32.9
	7	100.0	37.9	2.0	5.9	17.9	36.3
MCAox-HT	1	97.5	3.1	6.4	28.0	18.5	44.0
	2	99.9	31.2	1.8	2.4	19.2	45.4
	3	100.0	56.3	0.6	1.6	10.6	30.9
	4	99.9	64.2	0.7	1.0	9.0	25.1
	5	100.1	68.4	0.6	0.9	7.4	22.7
	6	100.0	69.8	0.8	1.6	7.6	20.2
	7	100.0	67.0	0.7	1.3	7.9	23.1
MCAox-MW	1	94.8	1.6	15.7	40.1	14.2	28.4
	2	99.3	18.9	4.1	3.9	21.0	52.1
	3	99.9	34.6	1.9	0.8	20.4	42.3
	4	100.0	48.6	2.0	1.2	17.5	30.8
	5	100.0	43.0	2.5	2.0	14.8	37.8
	6	99.7	50.3	1.6	2.0	13.4	32.8
	7	100.0	53.7	1.3	0.6	11.5	32.9

Catalyst	Reaction time (hr.)	%glycerol conversion	%selectivity				
			tri	1-mono	2-mono	1-3 di	1-2 di
Direct SBA-15-Pr-SO_3H	1	97.2	0.0	10.2	37.4	22.2	30.2
	2	98.5	4.9	8.3	15.3	32.1	39.4
	3	99.9	20.4	5.9	4.1	29.5	40.1
	4	100.0	42.2	1.5	0.9	25.4	30.0
	5	99.7	60.1	1.4	0.7	12.1	25.7
	6	99.9	65.0	1.1	0.5	15.3	18.1
	7	99.9	64.0	0.7	0.3	17.2	17.8

Reaction Condition: glycerol : oleic acid mole ratio 1:6, T = 110°C, 5 wt% of catalyst base on total reaction mixture